EOS MLS Cloud Ice Measurements and Cloudy-Sky Radiative Transfer Model

Dong L. Wu, Jonathan H. Jiang, and Cory P. Davis

***Abstract*— EOS MLS (Earth Observing System Microwave Limb Sounder) on the NASA Aura satellite observes upper tropospheric clouds at frequencies near 118, 190, 240, 640 GHz, and 2.5 THz. This paper describes MLS cloud measurement principles, the methods for cloud detection, and radiative transfer models used for interpreting and retrieving cloud properties. MLS 240 GHz data have been used to retrieve ice water content at pressures < 215 hPa. Some early results are shown here and the observed cloud effects are consistent with the expectation from model simulations in general. Significant cloud-induced radiances are observed at 2.5 THz. The cloud scattering signatures at 122 GHz are polarized but the polarization differences are typically less than 10% of the total cloud-induced radiance.**

***Index Terms*—satellite, microwave, cloud, limb sounding, ice water content, polarization**

I. Introduction

Clouds play important roles in modulating the Earth's dynamical, hydrological, radiative, and chemical processes [1,2,3,4]. Despite terabytes of satellite cloud imagery, our understanding of cloud properties and vertical distributions remain limited, especially on ice clouds in the upper troposphere. One of the poorly known cloud variables is ice water content (IWC), which is difficult to measure from space. Visible/IR techniques are sensitive only to the uppermost cloud layer and often saturated by dense clouds; whereas low-frequency microwave sensors are insensitive to most of ice clouds. To overcome both penetration and sensitivity shortcomings, high-frequency microwave radiometry emerges as a promising technique for observing ice clouds in the upper troposphere.

Manuscript received October 9, 2005. This work was performed at the Jet Propulsion Laboratory, California Institute of Technology, under contract with the National Aeronautics and Space Administration (NASA).

Dong L. Wu is with the Jet Propulsion Laboratory, California Institute of Technology, Pasadena, California, USA (phone: 818-393-1954; fax: 818-393-5065; e-mail: Dong.L.Wu@jpl.nasa.gov).

Jonathan H. Jiang is with the Jet Propulsion Laboratory, California Institute of Technology, Pasadena, California, USA (e-mail: Jonathan.H.Jiang@jpl.nasa.gov).

Cory P. Davis is with the Institute of Atmospheric and Environmental Science, School of GeoSciences, University of Edinburgh, Edinburgh EH9 3JZ, Scotland, UK. (e-mail: cdavis@staffmail.ed.ac.uk).

Remote sensing of ice clouds with passive microwave radiometers is a relatively new research area. A number of researchers have attempted to retrieve cloud ice water path (IWP) from nadir-viewing radiances using cloud scattering signatures [5,6,7,8,9]. Combined radar-radiometer approaches can be used to improve cloud ice measurements with better vertical resolution but the retrieved IWC profiles are limited to airborne radar sampling [10].

This paper describes a cloud ice observing technique with EOS MLS (Earth Observing System Microwave Limb Sounder) on Aura. Cloud radiance characteristics as well as measurement principles used for cloud ice retrievals are discussed. EOS MLS employs the limb-viewing technique with high-frequency narrow beamwidth receivers to achieve better vertical resolution and sensitivity than nadir sounding [11][12]. Under limb-viewing geometry the radiative transfer (RT) is greatly simplified, involving only the atmosphere and clouds. These advantages yield better accuracy for cloud detection at high altitudes.

Launched on 15 July 2004, EOS MLS has observed clouds in all the radiometers and is producing cloud IWC measurements at pressures < 215 hPa. Cloud IWC and horizontal ice water path (hIWP) along the instrument line-of-light (LOS) are two primary cloud products from EOS MLS [Figure 1]. The IWC in the upper troposphere (UT) is retrieved from high tangent height (h_t) single-frequency measurements assuming spherical homogeneity. This assumption implies that the MLS IWC represent a volume

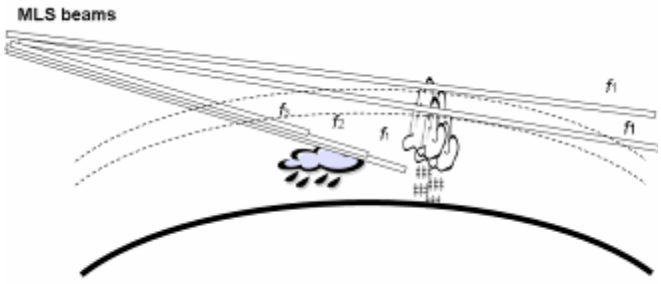

Figure 1. Cloud ice observations in limb viewing geometry. At high tangent heights, where limb radiation is optically thin for window channels, single-frequency radiances are used to retrieve IWC at pressures < 215 hPa. At low tangent heights, where limb radiation is optically thick, multiple frequency radiances with different penetration depths are used to infer hIWP along the LOS.

average over the instrument's field-of-view (FOV). The hIWP is retrieved from low-h_t measurements using multiple frequencies with different penetration depths. Each hIWP represents a column in the LOS direction that is nearly horizontally with an elevation angle of ~3º. In most cases the MLS hIWP column does not reach the surface due to strong atmospheric absorption along the limb path, but in the polar regions where air is often dry, the low-h_t radiances can reach the surface.

The retrieval technique using high-h_t radiances has previously applied to UARS (Upper Atmosphere Research Satellite) MLS 203 GHz data, from which the 100 hPa cloud ice was derived and studied for the period of 1991-1997 [13]. This work extends the cloud observing technique to EOS MLS frequencies, and the paper is organized to discuss cloud characteristics in EOS MLS radiances in section II, followed by a description of the cloudy-sky RT model in section III. Preliminary MLS cloud observations are highlighted in section IV.

II. EOS MLS Cloud Measurements

A. The EOS MLS Experiment

EOS MLS is a passive instrument that consists of seven radiometers at frequencies near 118, 190, 240, 640 GHz, and 2.5 THz [12][14]. There are dual polarizations for the 118 GHz and 2.5 THz receivers. Except for the 118 GHz radiometer, all are double-sideband receivers with key parameters specified in Table I. The GHz and THz systems have separate antennas but are synchronized in sampling such that they both produce 240 scans, or major frames (MAFs), in each orbit. Each MAF is further divided to 148 minor frames (MIFs). Unlike step-scanning with UARS MLS, EOS MLS scans are continuous in tangent height from the surface to the mesopause (~92 km) in 24.7s. Two adjacent scans are separated by ~165 km in distance. The latitude coverage ranges from 82ºS to 82ºN with a sun-synchronous ascending crossing time of ~1:40 p.m. Excluding instrument calibration, each MAF devotes ~120 MIFs for atmospheric measurements with a integration time of 1/6 second for a MIF. In the nominal operation [14], the GHz radiometers have ~42 MIFs dedicated to tropospheric measurements (separated by ~300 m in h_t), whereas the THz scan has only ~7 MIFs at h_t < 18 km [15].

Clouds reside mostly in the troposphere and occasionally shoot up to ~18 km. As a result, MLS radiances can be affected by clouds when viewing at h_t < ~19 km for the instrument FOV is not infinitesimal. The measured cloud fields are subject to substantial horizontal smearing due to a long (~200 km) limb path along the LOS.

B. Radiance Uncertainties

MLS clear-sky algorithms use radiance spectral variations to measure gas abundances, and therefore spectrally-flat radiance error has little impact on the quality of the gas measurements. The cloud measurements, however, depend critically on the absolute radiance value or accuracy of radiometric calibration. Thus, understanding noise accuracy is very important for reliable cloud retrieval. Noise characteristics and calibration issues are detailed in [14][15]. The radiance accuracy can be affected by several factors, including errors in baseline, gain, and sideband ratio. The baseline radiance may come from antenna's ohmic emissions and spillovers that can be removed effectively on a MAF-by-MAF basis, using the measurements at h_t > 85 km [14]. Although the gain is calibrated every MAF, it can be noisy and affected by the sidelope/spillover radiation not accounted for. The radiometer sideband ratios were measured during pre-launch testing but to the accuracy of 0.5-2%. The precision of MLS radiances consists of two components, frequency-correlated and random, which can be expressed in terms of variance as follows

Table I. Characteristics of the EOS MLS radiometers.
Both vertical and horizontal FOVs are estimated at h_t = 1 km.

MLS Radiometer[a] (frequency range in GHz)	Polarization 0º = V pol 90º = H pol	Estimated Min. Err[b] (K)	Vertical FOV (km)	Cross-Track FOV (km)
R1A (115-122)	0º ± 0.5º	0.3	6.5	13
R1B (115-122)	90º ± 0.5º	0.5	6.5	13
R2 (178-184, 200-207)	0º ± 0.5º	0.3	4.5	9
R3 (230-237, 243-250)	90º ± 0.5º	0.2	3.5	7
R4 (625-637, 649-661)	90º ± 0.5º	~2	1.5	3
R5H (2501-2515, 2531-2544)	~113º	~4	2.5	2.5
R5V (2501-2515, 2531-2544)	~23º	~3	2.5	2.5

a) The two frequency ranges in R2, R3, R4, R5H and R5V reflect the receiver's double-sideband coverage although radiances from two sidebands are inseparable in the radiometric measurements. R1A and R1B are single sideband radiometers with orthogonal polarizations.

b) MLS radiance error contains frequency-correlated and random components. The latter can be reduced by averaging radiances from different frequency channels with the radiometer but the correlated component cannot by reduced by averaging, eventually becoming the dominant radiance uncertainty. Values in this column, the minimum radiance error per MIF, reflect such limit after the frequency averaging is applied.

$$\sigma^2 = \sigma_{fc}^2 + \sigma_r^2 \quad (1)$$

where the random component σ_r^2 is proportional to the inverse of the bandwidth and integration time product. For cloud measurements, this part of noise can be averaged down with more channels (i.e., broader bandwidth). However, the frequency-correlated component, σ_{fc}^2, cannot be averaged down and becomes a fundament limitation to MLS ability in cloud detection. Especially for the 640 GHz and 2.5 THz radiances, such error can be as large as ~2 K and 3-4 K respectively, as indicated in Table I.

C. Cloud-induced radiances (Tcir)

The MLS filters are chosen to measure spectral line features from atmospheric gases (O_2, O_3, H_2O, N_2O, HNO_3, ClO, etc.). However, the frequencies useful for cloud measurements need to be away from these spectral lines so that the clear-sky and cloudy radiances can be better separated. Two criteria were used to choose the best window channels within each radiometer: 1) the lowest radiance in that radiometer at upper tropospheric h_t, and 2) the least correlation with the abundance of the above molecules. The radiances from the selected channels usually depend mostly on pointing and water vapor loading. However, for the 640 GHz measurements, O_3 and HNO_3 contributions (2-10 K) are present almost everywhere in all the MLS channels. Hence, the knowledge of H_2O, O_3 and HNO_3 distributions is also important for reliable cloud detection.

The basic cloud measurement is called cloud-induced radiance (*Tcir*), defined as the difference between the measured radiance and an estimated clear-sky background. The methods for the clear-sky background estimation are discussed in the next section. An example of the EOS MLS measurements is given in Fig. 2, where clouds can increase or decrease radiances depending on tangent height. At high high-h_t, where the radiances remain optically thin, *Tcir* are positive, in other words, providing more radiation relative to the clear-sky situation. In order to retrieve IWC from these high-h_t Tcir, we assume the spherical homogeneity for the cloud field and an IWC profile that decreases exponentially with height. Thus, the *Tcir* at high tangent heights is approximately proportional to IWC at the tangent height and can be converted using the modeled *Tcir*–IWC relations [13].

At low h_t, where limb radiances are optically thick, *Tcir* depends on hIWP as well as cloud position. In this case, clear-sky radiation can induce a *screening* effect, whereby air absorption in front of clouds attenuates the *Tcir* amplitude than the situation without the air absorption. This screening effect is clearly evident in the observed radiance spectra (Fig.2) where the cloudy-sky radiances at h_t = 4.7 km (red lines) produce the spectral line shapes that look like ones at a higher h_t. The occurrence of the spectral features (e.g., O_3) in cloudy atmospheres is because the emission near the line center comes mostly from the air above the cloud top, which

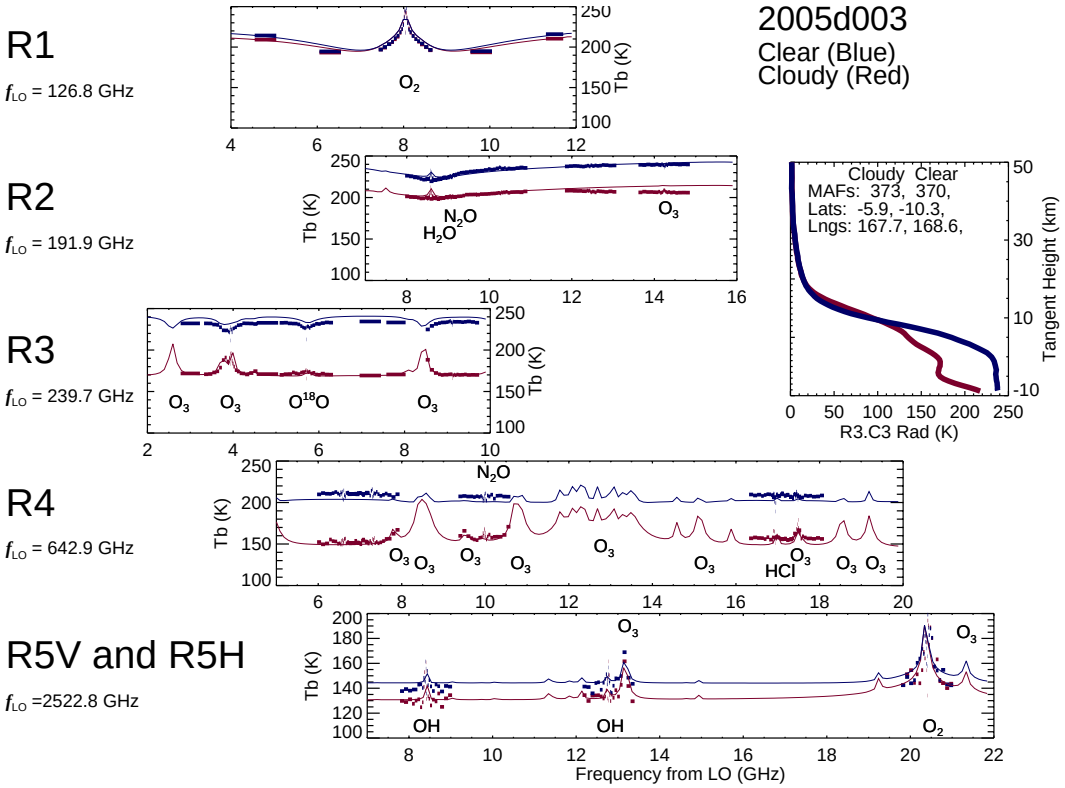

Figure 2. Measured (dotted lines) and modeled (continuous lines) radiance spectra for the EOS MLS radiometers at 4.7 km tangent height on 3 January 2005. Blue and red colors are two measurements at a close location but corresponding to clear and cloudy sky conditions. The right panel in the middle shows the measured radiance profiles from a 240 GHz window channel, where clouds depress radiances at low tangent heights but enhance them at high tangent heights.

becomes less affected by cloud scattering than those at the window channels. Thus, at these frequencies cloud scattering effects are as if a specular surface were brought up to the upper troposphere, where the radiance is a combination of reflected air emissions plus the surface emission. Because the *screening* effect is not modeled in MLS clear-sky forward model [16], cloudy radiances, if flagged as being affected, are either excluded or weighted less in the gas retrievals [17]. The cloud flag criteria are based on *Tcir*, which is re-evaluated at the end of each gas retrieval phase. Relatively loose criteria (i.e., cloudy if *Tcir* > 10 K or *Tcir* < -30 K) are currently implemented in the v1.5 algorithm (the first publicly available version of MLS data). Usually, the *Tcir* accuracy improves as the gas retrieval progresses in phase. The details on MLS retrieval phase design can be found elsewhere [17].

In MLS v1.5 algorithm, the *Tcir* used for the cloud ice retrieval is obtained after key molecules (e.g., H_2O, O_3, N_2O, and HNO_3) are retrieved. Then, the software uses the modeled *Tcir*-IWC and *Tcir*-hIWP relations (described in the following sections) to deduce IWC and hIWP. Thus, the accuracy of *Tcir* measurements directly affects the cloud ice retrievals, and several methods have been used for deriving reliable *Tcir* under different atmospheric conditions.

D. Methods for Tcir Calculations

Two methods have been used to obtain *Tcir*: empirical approach and radiative transfer (RT) model approach. The empirical approach takes advantage of differences in clear and cloudy sky variabilities (e.g., different spatial/temporal scales) to discriminate clear and cloudy components. The RT approach computes clear-sky radiance and interprets the unexplained radiance as *Tcir*. Both approaches have merits and work better than the other under certain circumstances. The empirical approach is simple and fast to implement, performing generally better in the region where atmospheric variability is small (e.g., in the tropics). The RT approach can adapt to large atmospheric variations (e.g. planetary waves at middle and high latitudes) but is computational expensive and affected by errors in auxiliary data (e.g., tangent pressure, temperature, water vapor).

As an empirical approach, the zonal mean radiances binned by latitude have been used satisfactorily as the background clear-sky radiance. Such zonal means are computed iteratively by discriminating outliers >3σ for each 10º latitude bin. The finalized zonal mean radiances are interpolated back onto the latitude of each individual measurement, and the difference between the measured radiance and the mean yields *Tcir*. A threshold, usually the 3σ from the mean, is used for determining cloud significance. The 3σ criterion is necessary to minimize the number of false alarms in cloud detection.

The RT method is used in the v1.5 algorithm for deriving *Tcir*. The MLS retrieval algorithm is designed to handle the tropospheric measurements with cautious and to improve *Tcir* calculations iteratively through progressive retrieval steps/phases. The phase for initial temperature (*T*) and tangent pressure (*P*) retrievals is very conservative and *does not* use any tropospheric radiance measurements so as to avoid potential cloud contaminations. The tropospheric *T* and *P* profiles in this phase are basically the a priori, the assimilation data from Global Modeling and Assimilation Office (GMAO) GEOS-4. Using these *T* and *P* profiles, *Tcir* is estimated by assuming 110% saturation in the troposphere. Cloud flags are generated with the loose criteria described in section II.C. The flagged radiances are still used in the H_2O retrieval phase that comes next but their precisions are inflated to 2 K. After the H_2O is retrieved, *Tcir* are re-evaluated and cloud flags are re-generated for radiances in each radiometer. Cloudy radiances are either weight less or excluded in the subsequent gas retrievals, and *Tcir* are finalized after the key molecules (e.g., H_2O, O_3, N_2O, and HNO_3) are retrieved.

III. Cloudy-Sky RT Models

A. Radiative Transfer Equation

The cloudy-sky RT equation can be expressed as the differential change of radiance with respect to distance interval *ds* in the radio wave propagation direction **n**:

$$\frac{d\mathbf{I}(\mathbf{n})}{ds} = -\mathbf{K}(\mathbf{n})\mathbf{I}(\mathbf{n}) + \mathbf{k_a}(\mathbf{n})B(T) + \oint_{4\pi}\mathbf{P}(\mathbf{n},\mathbf{n}')\mathbf{I}(\mathbf{n}')d\mathbf{n}' \quad (2)$$

where $\mathbf{I}=[I,Q,U,V]^T$ is the Stokes vector in $Wm^{-2}\mu m^{-1}sr^{-1}$, *s* is the distance along direction **n,** and *B* is Planck radiance at air temperature *T*. $\mathbf{K}(\mathbf{n})$, $\mathbf{k_a}(\mathbf{n})$, and $\mathbf{P}(\mathbf{n},\mathbf{n}')$ are, respectively, the bulk extinction matrix, absorption coefficient vector and scattering matrix of the medium. For brevity these variables have been expressed as bulk properties, where individual single scattering properties have been multiplied by particle number density and averaged over all orientations and particle types. The argument **n** has been retained to signify that in general these properties depend on the direction of propagation.

Cloud scattering greatly complicates the RT problem. The last term in Eq. (2) means that for a single LOS calculation, knowledge of the whole radiation field is required. Also, a thorough treatment of scattering requires the consideration of polarization, which transforms the RT equation from a scalar equation in the clear-sky case to the vector equation above.

To thoroughly investigate the influence of clouds on MLS radiances, a 3D polarized radiance model, ARTS (Atmospheric Radiative Transfer System), is used for MLS simulations [18]. In this 3D RT model, a reversed Monte Carlo technique is employed to track back random multiple scattered propagation paths from the sensor to either the emitting point or the entry into the scattering domain. To date, this model has only been used as a reference for comparison to the simplified model described below, and for interpretation of polarized MLS measurements [19].

B. MLS Cloud-Sky Forward Model

For cloud retrievals it is desirable to minimize the computational expense of the RT model (hereafter referred as to *the forward model*). This section describes the operational

forward model, where several approximations have been made to Eq. (2) to simplify scattering computation.

First, we neglect polarization differences in the radiation, i.e., $\{Q, U, V\} \approx 0$. This reduces Eq (2) to

$$\frac{dI}{ds} = -\beta_e I + \beta_a B(T) + \beta_s J_s \tag{3}$$

where $\beta_e \equiv \beta_{gas\_a} + \beta_{c\_s} + \beta_{c\_a}$ denotes volume extinction coefficient, which includes contributions from gas absorption (β_{gas_a}), cloud scattering and absorption (β_{c_s} and β_{c_a}). The source function J_s, representing the amount of radiation scattered-in by clouds, is an angular integration of radiation over all incident directions.

Using the Rayleigh-Jeans approximation, it is convenient at microwave frequencies to transform radiance to more measurement-related variables by defining

$$\hat{T} \equiv \frac{c^2}{2k\nu^2} B$$

$$T_b \equiv \frac{c^2}{2k\nu^2} I$$

where $\hat{T}$ and T_b have unit of *Kelvin* (K). T_b is also called radiance brightness temperature. Similarly, the scattering source function J_s is replaced by T_{scat} , which is defined as:

$$T_{scat} \equiv \frac{1}{4\pi} \oint P(\Omega, \Omega') T_b(\Omega') d\Omega' \tag{4}$$

where Ω is the solid angle of radiation coming out of clouds, and Ω' is the solid angle of incident radiation. The difference

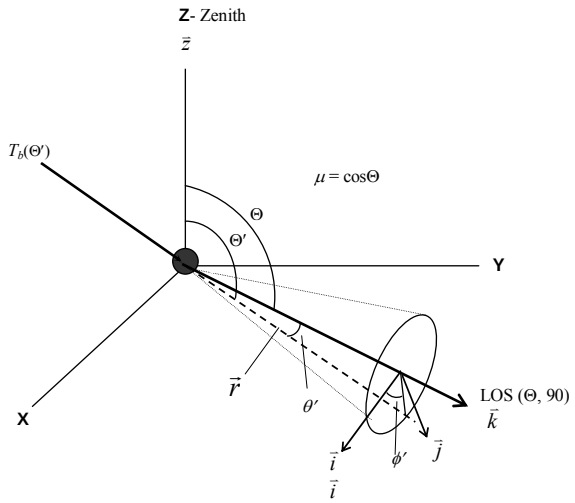

Figure 3: Diagram illustrating the scattering in a spherical geometry, where the Z-axis is at the zenith. The origin is a differential volume containing polydisperse particles, and the LOS lies in the Y-Z plane with an angle Θ with respect to zenith and an angle Φ=90° with respect to X. The (θ, ϕ) coordinates are relative to the LOS. ϕ' is the azimuth angle that lies in the plane perpendicular to the LOS.

between Ω and Ω' is the scattering angle.

Figure 3 illustrates the geometry used for the T_{scat} calculation. The plane-parallel assumption is made to simplify the scattering calculation such that incident radiance T_b at zenith angle Θ', a function of θ, ϕ, and Θ, can be reduced to a function of single variable Θ' , i.e.,

$$T_{scat}(\Theta) = \frac{1}{2} \int_0^{\pi} P(\theta') \overline{T}_b(\theta') \sin\theta' d\theta' \tag{4}$$

and

$$\overline{T}_b(\theta') = \frac{1}{2\pi} \int_0^{2\pi} T_b(\Theta') d\phi' \tag{5}$$

where Θ' is related to θ', ϕ' and Θ by

$$\cos\Theta' = \vec{r} \cdot \vec{z} = \sin\theta' \sin\Theta \sin\phi' + \cos\theta' \cos\Theta \tag{6}$$

If we use optical thickness $d\tau = \beta_e \cdot \mu \cdot ds$ (where $\mu = \cos\Theta$) as the path coordinate, Eq. (3) can be further reduced to:

$$\mu \frac{dT_b(\mu, \tau)}{d\tau} = -T_b(\mu, \tau) + (1 - \omega_0)\hat{T}(\tau) + \omega_0 T_{scat} \tag{7}$$

where ω_0 is the *single scattering albedo* characterizing the relative importance of scattering and emission contributions in the atmosphere. The source function T_{scat} is solved iteratively from Eq. (7) under the plane-parallel assumption. The iterative approach works as follows. For a given set of scattering

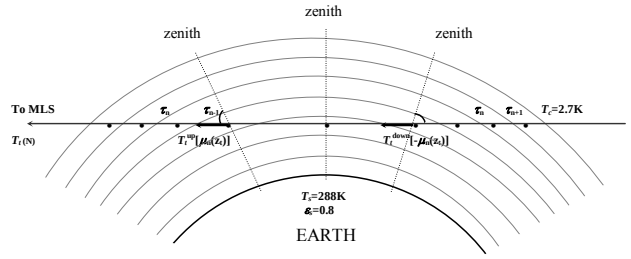

Figure 4: Geometry for limb-viewing radiative transfer calculations.

angles, in each model layer we first compute T_{scat} from Eq.(4-5) using clear-sky radiances, and then solve the new set of radiances using Eq.(7). Because the new radiances may differ from the clear-sky radiances, we need to re-evaluate T_{scat} from Eq.(4-5), and use Eq.(7) to solve for the radiances at each layer again. The number of iterations depends on the disturbance created by cloud scattering, the stronger scattering the more iterations are needed. Usually, convergence (<0.1 K in radiance differences), or the solution for T_{scat}, can be found within 3-10 iterations. Once the T_{scat} solution is obtained, we may calculate radiation along any path using Eq.(7) with T_{scat} projected onto the path direction. One of the most interesting path is the MLS LOS, along which the radiance is computed by integrating Eq. (7) from cold space, through an atmospheric limb, to MLS [Figure 4].

C. Polydispersion of Ice Crystals

Cloud volume scattering and absorption coefficients are determined by a polydispersion of particles with number density $N(r)$ as a function of mass-equivalent particle radius r. We assume all spherical particles in the cloud, an approximation for random orientation of particles. $N(r)$ is referred hereafter as to particle size distribution (PSD). The volume extinction and scattering coefficients (β_{c_s} and β_{c_a}) from the cloud, therefore, are the sums over all the single particle contributions, namely

$$\beta_{c\_e} = \pi \int_0^{\infty} N(r) r^2 \xi_e(r) dr \tag{8}$$

$$\beta_{c\_s} = \pi \int_0^{\infty} N(r) r^2 \xi_s(r) dr \tag{9}$$

where (ξ_e, ξ_s) are single particle extinction and scattering efficiencies from the Mie solution. The ice and water permittivities, as described in [20], are based on laboratory measurements and parameterized as a function of temperature and frequency. The volume absorption coefficient can be obtained from the difference, namely

$$\beta_{c\_a} = \beta_{c\_e} - \beta_{c\_s}. \tag{10}$$

Similarly, the phase function of cloud scattering in polydispersion is the integration over all particle sizes:

$$P(\theta) = \frac{\pi}{\beta_{c\_s}} \int_0^\infty N(r) r^2 \xi_s(r) p(\theta, r) dr \tag{11}$$

where θ is the scattering angle, and $p(\theta,r)$ is the phase function of single size particle from the Mie solution. To link scattering properties with cloud ice, we use a parameterized PSD [21], which is a function of temperature and IWC, based on in-situ measurements. Particle sizes are divided into 40 bins between 0-4000 μm in diameter. To characterize the PSD properties, IWC, mass-mean diameter (D_{mm}), and effective diameter (D_e) are often used and they are defined by

$$IWC \equiv \frac{4}{3} \pi \rho_i \int_0^\infty N(r) r^3 dr \tag{12}$$

$$D_{mm} \equiv \int_0^\infty N(r) r^4 dr \Big/ \int_0^\infty N(r) r^3 dr \tag{13}$$

$$D_e \equiv \int_0^\infty N(r) r^3 dr \Big/ \int_0^\infty N(r) r^2 dr \tag{14}$$

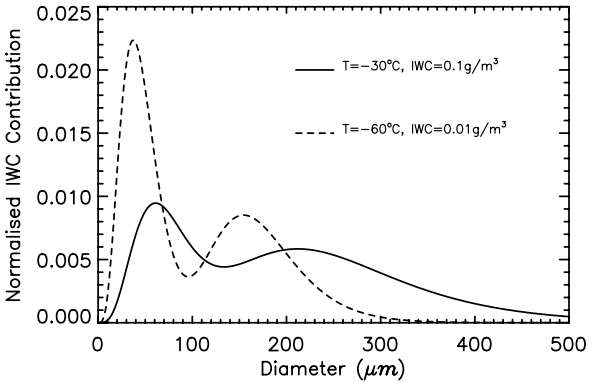

Figure 5. IWC contributions weighted by the parameterized PSD [21]. It shows relative importance of contributions from different particle sizes. The distributions are normalized such that the area under these curves is unity. Two cloud examples are characterized by: IWC=0.01g/m^3, –60°C and IWC=0.1g/m^3, –30°C. The double peaks reflect the bimodal size distributions in the PSD [21].

Ice clouds may have a bimodal PSD in the upper troposphere [Fig. 5]. The PSD used the RT model serves as the key assumption to relate single-frequency measurements to the total ice mass. For example, the 240 GHz radiances are mostly sensitive to the large-size mode in Fig.5 whereas the 640 GHz sensitivities to the two modes are about equal. By comparing MLS observations at these frequencies, one can infer some particle size information about the cloud.

D. Modeled Tcir-IWC and Tcir-hIWP Relations

The modeled *Tcir*-IWC and *Tcir*-hIWP relations are used to produce a fast IWC retrieval. At high h_t we use the limb radiances that are still optically thin, where *Tcir* increases approximately linearly with IWC for IWC < ~30 mg/m^3 at 240 GHz [Fig. 6] and < ~5 mg/m^3 at 640 GHz. Because the clear-sky forward model is too computationally costly to implement, the pre-calculated *Tcir*-IWC coefficients provide the first-order retrieval for IWC. To calculate these

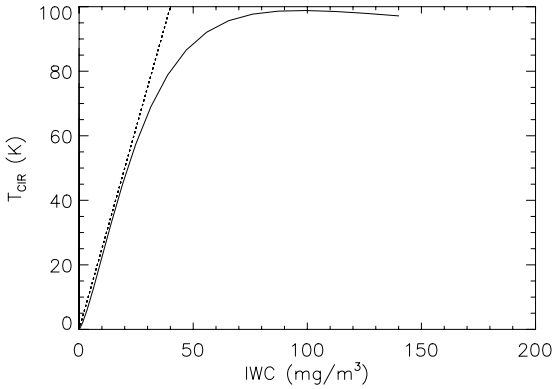

Figure 6. Modeled Tcir-IWC relation for 240 GHz limb radiance at 100 hPa. The dotted line shows the linear portion of the relation with a slope of 0.4 mg/m^3/K, and saturation occurs at ~50 mg.

coefficients we use the MF97 PSD and the CIRA86 (COSPAR International Reference Atmosphere 1986) tropical temperature profile [22]. Table II lists the *Tcir*-to-IWC conversion coefficients calculated with MLS v1.5 software, as a function of frequency and tangent pressure. More sophisticated *Tcir*-IWC relations, such as latitude-dependent coefficients under different clear-sky backgrounds, can be developed if needed. At present, uncertainty in the *Tcir*-IWC relation is dominated by the PSD parameterization and particle shape assumption used for ice clouds [21]. Dependence of PSD on latitude and effects of mixed-phase clouds are neglected. Different PSDs could yield a factor of 2-3 differences in the deduced IWC. Clouds with very large IWC can make the *Tcir*-IWC relations deviate from the linearity but these cases represent a very small percentage of MLS cloud measurements.

The *Tcir*-to-*hIWP* conversion coefficients are calculated for the same atmospheric profiles as for the *Tcir*-IWC calculations, and the results are given in Table III. The MLS *hIWP* is defined by

$$hIWP \equiv \int_{LOS} IWC(s) e^{-\tau_e(s)} ds \tag{15}$$

where $\tau_e(s) = \int_{LOS}^{s} \beta_e(s') ds'$ is the frequency-dependent optical depth along LOS. The weight $e^{-\tau_e(s)}$ is also known as the transmission function, which determines the percentage of IWC(s) observable by the instrument at this location. In this

definition, hIWP excludes the contributions beyond extinction, and radiances with different penetration depths will yield different hIWPs even for the same cloud [Fig. 1].

Table II: Calculated coefficients (mg/m^3/K) for the *Tcir-IWC* relations for high tangent heights

Ptan hPa	190 GHz	240 GHz	640 GHz
68	0.5	0.40	0.14
83	0.5	0.40	0.14
100	0.8	0.40	0.23
121	1.4	0.43	-
147	1.9	0.61	-
178	-	0.86	-
215	-	1.0	-

Table III: Calculated coefficients (g/m^2/K) for the *Tcir-hIWP* relations for low tangent heights

Radiometer		Coefficients		
Freq	(GHz)	h_t=1km	h_t=5km	h_t=10km
R1A	115.3	-588	-682	-1850
	122.0	-3000	-3380	-4570
R2	177.0	-86.2	-90.1	-
	200.5	-46.7	-47.8	-
R3	233.0	-28.2	-29.3	-
	245.4	-23.9	-24.8	-
R4	636.5	-1.69	-1.74	-1.93
	649.5	-2.70	-1.72	-1.92
R5V	2514.8	-0.41	-0.41	-0.43
	2530.8	-0.41	-0.41	-0.43

IV. Early Results from EOS MLS

A. IWC Retrieval

The EOS MLS standard IWC product in v1.5 comes from the 240 GHz measurements where the radiance is affected least by atmospheric gas and continuum emissions. In the IWC retrieval, we first retrieve a quantity called *baseline*, a spectrally-flat radiance component, for each MIF by constraining key gas molecules (e.g., H_2O, O_3, N_2O, and HNO_3) to their retrieved values [17]. Thus, the retrieved baseline can be viewed as the radiance not explained by the clear-sky forward model used in the retrieval, and we interpret it as *Tcir*. Secondly, we use the modeled *Tcir*-IWC coefficients to obtain IWC for pressure levels > 215 hPa.

Shown in Figure 7 are the distributions of retrieved IWC during 9-11 January 2005. Only significant (> 5 mg/m^3) cloud measurements are shown in colors. The threshold for significant IWC varies from 5 mg/m^3 at 100 hPa to ~10 mg/m^3 at 215 hPa. The cloud detection threshold depends critically on the accuracy of the clear-sky RT model, and on how well all the gaseous contributions are measured and modeled.

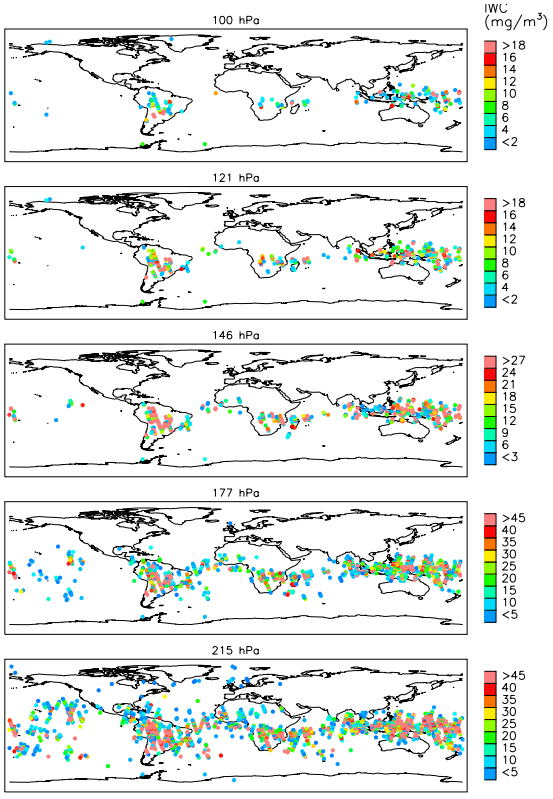

Figure 7. Composite maps of MLS IWC measurements during 9-11 January 2005.

B. MLS 240 and 640 GHz Tcir

Simultaneous MLS 240 and 640 GHz measurements have been used to distinguish clouds with different PSDs. Fig. 8a shows the 640 GHz *Tcir* on 29 August 2004 when strong enhancements in dense cirrus are found over Asia at altitudes > 14 km [22]. These *Tcir* are derived with the empirical method as discussed in section II.B using the zonal mean radiance for the clear-sky background.

The 640 GHz clear-sky radiance is typically ~140 K at 15 km tangent height mainly due to atmospheric continuum radiation. As given in Table I, the 640 GHz radiometer has a relatively large frequency-correlated error, which cannot be averaged out. Thus, a large threshold (10 K) is used for cloud detection, which corresponds to the ~3σ variability about the background. At 240 GHz the clear-sky background is ~20 K with the 3σ variability of ~5 K.

RT calculations (Fig. 8b) show that the 240:640 GHz correlation is quite sensitive to the cloud PSD. D_{mm} serves as a better parameter than D_e to characterize the PSD differences since D_e varies only slightly among these clouds. D_e has been widely used in visible/IR cloud retrievals because of their sensitivity to scattering cross-section on the uppermost cloud layer. At microwave frequencies, the small-D_{mm} cloud scattering can be neglected and the 240:640 GHz correlation virtually exhibits a ratio similar to clear-sky measurements. For clouds with large D_{mm}, scattering becomes important, but

unlike visible/IR techniques, it is related to volume scattering of ice particles.

An interesting and useful property at 15 km tangent height

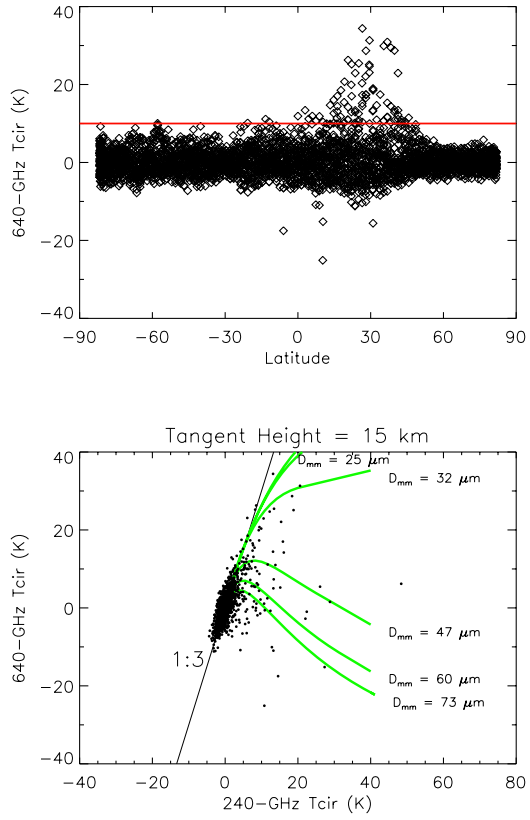

Figure 8. (a) MLS 640 GHz *Tcir* at 15 km tangent height for 29 August 2004. (b) Correlation between 240 and 640 GHz *Tcir* at 15 km tangent height for the same day. The curves are the model 240:640 GHz relations with various D_{mm} labeled on the side.

is that the 640 GHz radiance becomes insensitive to cloud scattering because of the large (~140 K) clear-sky background. Under this background, the amounts of scattered-in and scattered-out radiation are approximately equal, making the net 640 GHz *Tcir* about zero. On the other hand, the 240 GHz sensitivity to large D_{mm} clouds remains excellent because of the small (~20 K) clear-sky screening at this height. These sensitivity differences allow MLS to distinguish upper-tropospheric clouds of different D_{mm}.

C. MLS and NASA's "A-Train" Satellite Measurements

Known having large spatial and temporal variabilities, clouds are generally undersampled by a single instrument or a single platform. As part of NASA synergic observing system, the *A-Train*, Aura is flying in formation with Aqua (launched in 2002), and CloudSat 94-GHz Cloud Profiling Radar (CPR) (due for launch in 2005) [24] with coincident measurements within ~15 and ~7 min, respectively. Aqua AIRS (Atmospheric Infrared Sounder) [25] and MODIS (Moderate Resolution Imaging Spectroradiometer) [26] provide high-resolution horizontal coverage at visible and infrared frequencies whereas the CloudSat CPR will provide high vertical resolutions of cloud ice profiles. Together with these *A-Train* observations, the MLS 118 GHz – 2.5 THz radiances can provide more insights on cloud properties and variabilities. As illustrated in Fig. 9, MLS radiances exhibit large variability in cloudy regions where the IR radiances saturate.

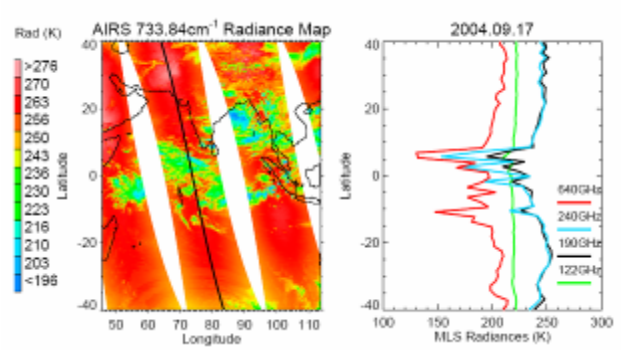

Figure 9. An example of the A-Train cloudy radiances observed by Aqua AIRS (left) and Aura MLS (right). The straight line in the center of AIRS swath is the MLS measurement track for 17 September 2004. The AIRS channel (733.84 cm^{-1}) has a clear-sky weighting function peaked at ~800 hPa, whereas the MLS weighting functions at 122, 190, 240 and 640 GHz window channels peak at about 170, 270, 270, and 200 hPa, respectively.

D. THz Tcir

Despite strong atmospheric continuum absorption at 2.5 THz, the THz frequency channels in spectral windows can penetrate down to the upper troposphere and still be sensitive to clouds. Like the 640 GHz radiances, the THz measurements have a relatively large correlated noise that cannot be reduced by frequency averaging. As listed in Table I, the minimum precision for the THz radiances is ~3-4 K, corresponding to 9-12 K in 3σ uncertainty. This largely limits the THz sensitivity to clouds, especially to cirrus clouds of small IWC. Nevertheless, as shown in Fig. 10, *Tcir* as large as -30 K are

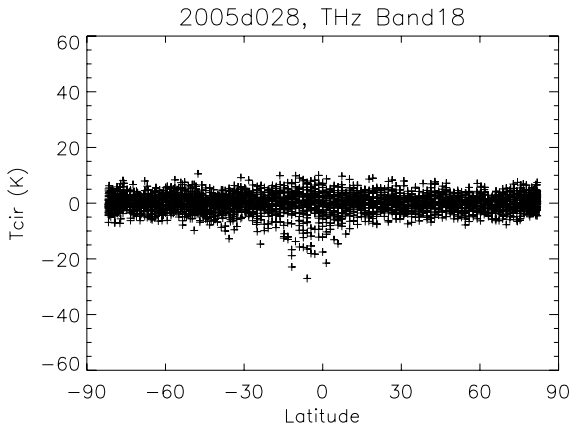

Figure 10. *Tcir* on 28 January 2005, derived from the band 18 radiances in the 2.5 THz radiometer for h_t < 5 km. Cloud scattering cause the observed radiances less than typical clear-sky backgrounds, producing negative *Tcir*, where measurements with *Tcir* < -10 K indicate the significant presence of clouds.

observed due to scattering of ice clouds at high altitudes. These *Tcir* measurements in the tropics represent a mixture of dense cirrus and deep convective clouds.

E. Polarized Tcir at 122 GHz

The R1A(H) and R1B(V) radiometers in EOS MLS have the same frequency channels but measure radiation with orthogonal polarizations. The 122 GHz radiances at h_t < 10 km can penetrate into the upper troposphere and be affected by cloud scattering. In strong deep convection cases, *Tcir* can reach -40 K, and the polarization difference between R1A and R1B *Tcir* can be as large as 4 K due to orientation preference of ice crystals, as shown in Fig. 11. The polarization difference in the 122 GHz radiances is typically < 10% of the *Tcir* value. A detailed analysis and modeling study on the MLS R1A and R1B polarized radiances can be found elsewhere [19].

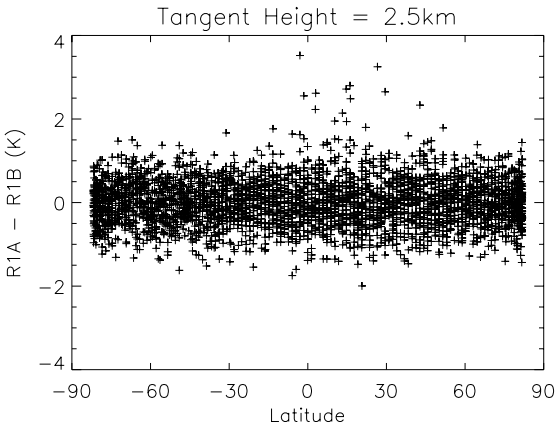

Figure 11. R1A-R1B radiance differences at 2.5 km tangent height for 29 August 2004. The positive differences indicate that *Tcir* at 122 GHz are polarized due to preferential orientation of ice crystals. The polarization differences can be as high as 4 K, significantly above the 3σ noise background (~1.5 K).

V. SUMMARY AND FUTURE WORK

We have described the methods used to derive MLS *Tcir* with examples from recent measurements. These methods continue to be refined as the MLS radiances are better understood and modeled. A cloudy-sky RT model is used to retrieve IWC at pressures < 215 hPa and the hIWP along MLS LOS at h_t < 5 km. The model assumes realistic PSDs based on in-situ measurements and computes the *Tcir*-IWC and *Tcir*-hIWP relations as a function of frequency and tangent height.

Preliminary results from the Aura MLS indicate that the 240 GHz radiances provide useful IWC measurements. The retrieved IWC distribution in the upper troposphere represents realistic cloud climatology. In addition, the THz radiances at low h_t are found to be sensitive to cloud scattering, where *Tcir* can reach -30 K. At 122 GHz, significant (3-4 K) polarized cloud radiances are observed and the polarized signals are typically < 10% of total *Tcir*.

The hIWP retrievals are currently under development and will be implemented in a future version of MLS algorithms. The MLS channels near the 183.3 GHz water line and the 233.9 GHz $O^{18}O$ line can provide multiple hIWP*s* with different penetration depths, from which we can derive *IWC* in several layers. These cloud ice measurements, averaged over MLS LOS, can be compared with other *A-Train* observations, such as those from CloudSat CPR, to further reduce cloud ice uncertainty.

ACKNOWLEDGMENT

This work was performed at the Jet Propulsion Laboratory, California Institute of Technology, under contract with the National Aeronautics and Space Administration (NASA). We thank the Aura project for supporting this work and our MLS colleagues for the instrument operation and data processing, especially Joe Waters, William Read and Mark Filipiak for valuable discussions on this work.

REFERENCES

[1] V. Ramanathan, R. D. Cess, E. F. Harrison, et al., Cloud-radiative forcing and climate - results from the Earth radiation budget experiment. *Science* **243**, 57-63, 1989.

[2] G. L. Stephens, Cloud feedbacks in the climate system: A critical review, *J. Climate*, **18**, 237-273, 2005.

[3] B. A. Wielicki, R. D. Cess, M. D. King, D. A. Randall, and E. F. Harrison, 1995: Mission to planet Earth: Role of clouds and radiation in climate. Bull. Amer. Meteor. Soc., 76, 2125–2153.

[4] R. D. Cess, and Coauthors, 1989: Interpretation of cloud climate feedback is produced by 14 atmospheric general circulation models. Science, 245, 513–516.

[5] J. Vivekanandan, J. Turk, and V. N. Bringi, Ice water path estimation and characterization using passive microwave radiometry. *J. Appl. Meteor.*, **30**, 1407-1421, 1991.

[6] A. J. Gasiewski, Numerical sensitivity analysis of passive EHF and SMMW channels to tropospheric water vapor, clouds, and precipitation. *IEEE Trans. Geosci. Remote Sens*., **30**, 859-870, 1992.

[7] K. F. Evans and G. L. Stephens, Microwave radiative transfer through clouds composed of realistically shaped ice crystals. Part II: Remote sensing of ice clouds. *J. Atmos. Sci.*, **52**, 2058-2072, 1995.

[8] G. Liu, and J. A. Curry, Topical ice water amount and its relations to other atmospheric hydrological parameters as inferred from satellite data. *J. Appl. Meteor.*, **38**, 1182-1194, 1998.

[9] F. Weng, and N. C. Grody, Retrieval of ice cloud parameters using a microwave imaging radiometer. *J. Atmos. Sci.*, **57**, 1069-1081, 2000.

[10] G. M. Skofronick-Jackson, and J. R. Wang, The estimation of hydrometeor profiles from wideband microwave observations. *J. Appl. Meteor.*, **39**, 1645-1656, 2000.

[11] J. W. Waters, et al., " The UARS and EOS Microwave Limb Sounder Experiments," *J. Atmos. Sci.*, **56** pp. 194-218, 1999.

[12] J. W. Waters, et al., "The Earth Observing System

Microwave Limb Sounder (EOS MLS) on the Aura Satellite," *IEEE Trans. on Geoscience and Remote Sensing*, this issue.

[13] D. L. Wu, and coauthors, "UARS MLS Cloud Ice Measurements and Implications for H_2O Transport near the Tropopause," *J. Atmos. Sci.*, in press, 2005.

[14] R. F. Jarnot, M. J. Schwartz, et al., "Radiometeric and spectral performance and calibrations of the GHz band on Aura MLS," *IEEE Trans. on Geoscience and Remote Sensing*, this issue.

[15] H. M. Pickett, "Microwave Limb Sounder THz module on Aura," *IEEE Trans. on Geoscience and Remote Sensing*, this issue.

[16] W. G. Read, Z. Shippony, M. J. Schwartz, and W. V. Snyder, "The clear-sky unpolarized forward model for the EOS Aura Microwave Limb Sounder (MLS)," *IEEE Trans. on Geoscience and Remote Sensing*, this issue.

[17] N. J. Livesey and W. V. Snyder, "Retrieval algorithms for the EOS Microwave Limb Sounder," *IEEE Trans. on Geoscience and Remote Sensing*, this issue.

[18] C. P. Davis, C. Emde, R. Harwood, "A 3D Polarized Reversed Monte Carlo Radiative Transfer Model for mm and sub-mm Passive Remote Sensing in Cloudy Atmospheres," *IEEE Trans. on Geoscience and Remote Sensing*, in press, 2005.

[19] C. P. Davis, D. L. Wu, C. Emde, J. H. Jiang, R. E. Cofield, and R. S. Harwood, "Cirrus Induced Polarization in 122 GHz Aura Microwave Limb Sounder Radiances", J. Geophys. Res. Lett., in review, 2005b.

[20] J. H. Jiang, and D. L. Wu, "Ice and Water Permittivities for Millimeter and Sub-millimeter Remote Sensing Applications," *Atmospheric Science Letters*, **5**(7), 146-151, 2004.

[21] G. M. McFarquhar and A. J. Heymsfield, Parameterization of tropical cirrus ice crystal size distributions and implications for radiative transfer: Results from CEPEX. *J. Atmos. Sci*., **54**, 2187-2200, 1997.

[22] E. S. Fleming, et al., 1990. Zonal mean temperature, pressure, zonal wind, and geopotential height as function of latitude. Adv. Space Res., 10, 11-59.

[23] D. L. Wu and coauthors, Variations of Upper Tropospheric Clouds and Pollution over Asia: Recent Observations by MLS on Aura, in preparation, 2005.

[24] G. L. Stephens and coauthors, The CloudSat Mission and the A-Train: A new dimension of space-based observations of clouds and precipitation. *Bull. Amer. Meteor. Soc.*, **83**(12), 1771-1790.

[25] H. H. Aumann and coauthors, "AIRS/AMSU/HSB on the Aqua Mission: Design, Science Objectives, Data Products, and Processing Systems." *IEEE Trans. on Geoscience and Remote Sensing*, **41** #2, 253-264, 2003.

[26] S. Platnick and coauthors, "The MODIS cloud products: Algorithms and examples from Terra. IEEE Trans. on Geoscience and Remote Sensing," **41**, 459-473, 2003.

Dong L. Wu (M'96) received B.S in 1985 from University of Science and Technology of China, M.S. in physics from the Louisiana State University in 1990, M.S. in electrical engineering and Ph.D. in atmospheric science in 1993 and 1994 from the University of Michigan.

He joined the Jet Propulsion Laboratory, California Institute of Technology, Pasadena, California in 1994 to conduct data analyses and algorithm development for the MLS project, and currently is a co-investigator of the EOS MLS experiment. He has authored and coauthored more than 45 papers in peer-reviewed journals on subjects in atmospheric clouds and small-scale gravity waves. He received JPL Excellence Award in 1997 and NASA Exceptional Achievement Medal in 2001.

Jonathan H. Jiang received B.Sc. in Astrophysics in 1985 at Beijing Normal University. He earned his M.Sc. in Astrophysics in 1991 and Ph.D. in Atmospheric Physics in 1996, both at York University in Canada. Early in his career in 1986-1988, he taught physics and astronomy at Nanjing Institute of Technology in China. He later worked at Canada's Space Astrophysics Laboratory of Institute for Space and Terrestrial Science in 1989-1991, and Centre for Research in Earth and Space Science at York University in 1992-1995, where he was involved, respectively, in the International Ultraviolet Explorer satellite mission and the Canadian Middle Atmospheric Model project. Between 1996-2001, he was on research staff and post-doctoral fellowships at McGill's Centre for Climate and Global Change Research, University of Quebec at Montreal, and California Institute of Technology, and held two part-time physics teaching positions at Trent University and University of Waterloo while in Canada. He joined the Jet Propulsion Laboratory in 1999, and is currently a research scientist working for the EOS MLS project. His primarily research interest is radiative transfer modeling, detection of clouds at microwave frequencies and application of MLS data in climate models.

Cory Davis received the degrees of BSc (Hons,1) and Ph. D. in physics at the University of Otago, Dunedin, New Zealand, in 1996 and 2001 respectively. Currently he is a post-doctoral research fellow the Institute for Atmospheric and Environmental Science at the University of Edinburgh, Scotland. Dr. Davis is a member of the Microwave Limb Sounding team at this institute, and is funded under the NERC Clouds, Water Vapour and Climate (CWVC) thematic program. His primarily research interest is the influence of Cirrus on EOS-MLS trace gas and cloud property retrievals.